

# Cotargeting Polo-Like Kinase 1 and the Wnt/ $\beta$ -Catenin Signaling Pathway in Castration-Resistant Prostate Cancer

Jie Li,<sup>a</sup> Anju Karki,<sup>b</sup> Kurt B. Hodges,<sup>c</sup> Nihal Ahmad,<sup>d</sup> Amina Zoubeidi,<sup>e</sup> Klaus Strebhardt,<sup>f</sup> Timothy L. Ratliff,<sup>g</sup> Stephen F. Konieczny,<sup>b,g</sup> Xiaoqi Liu<sup>a,g</sup>

Department of Biochemistry, Purdue University, West Lafayette, Indiana, USA<sup>a</sup>; Department of Biological Science, Purdue University, West Lafayette, Indiana, USA<sup>b</sup>; Department of Pathology and Laboratory Medicine, Indiana University School of Medicine, Indianapolis, Indiana, USA<sup>c</sup>; Department of Dermatology, University of Wisconsin, Madison, Madison, Wisconsin, USA<sup>d</sup>; The Vancouver Prostate Centre, Vancouver, British Columbia, Canada<sup>e</sup>; Department of Obstetrics and Gynecology, J. W. Goethe University, Frankfurt, Germany<sup>f</sup>; Center for Cancer Research, Purdue University, West Lafayette, Indiana, USA<sup>g</sup>

**The Wnt/ $\beta$ -catenin signaling pathway has been identified as one of the predominantly upregulated pathways in castration-resistant prostate cancer (CRPC). However, whether targeting the  $\beta$ -catenin pathway will prove effective as a CRPC treatment remains unknown. Polo-like kinase 1 (Plk1) is a critical regulator in many cell cycle events, and its level is significantly elevated upon castration of mice carrying xenograft prostate tumors. Indeed, inhibition of Plk1 has been shown to inhibit tumor growth in several *in vivo* studies. Here, we show that Plk1 is a negative regulator of Wnt/ $\beta$ -catenin signaling. Plk1 inhibition or depletion enhances the level of cytosolic and nuclear  $\beta$ -catenin in human prostate cancer cells. Furthermore, inhibition of Wnt/ $\beta$ -catenin signaling significantly potentiates the antineoplastic activity of the Plk1 inhibitor BI2536 in both cultured prostate cancer cells and CRPC xenograft tumors. Mechanistically, axin2, a negative regulator of the  $\beta$ -catenin pathway, serves as a substrate of Plk1, and Plk1 phosphorylation of axin2 facilitates the degradation of  $\beta$ -catenin by enhancing binding between glycogen synthase kinase 3 $\beta$  (GSK3 $\beta$ ) and  $\beta$ -catenin. Plk1-phosphorylated axin2 also exhibits resistance to Cdc20-mediated degradation. Overall, this study identifies a novel Plk1-Wnt signaling axis in prostate cancer, offering a promising new therapeutic option to treat CRPC.**

Prostate cancer (PCa) is the most diagnosed malignant neoplasm of males in the Western world, with men having a 1-in-6 chance of developing invasive PCa within their lifetime in the United States. The androgen receptor (AR) signaling pathway, which is essential for the growth of PCa cells, including late-stage castration-resistant prostate cancer (CRPC), is a valid therapeutic target for PCa patients (1). Current approaches to treat CRPC are to delay or replace treatment with cytotoxic agents (e.g., docetaxel) with androgen signaling inhibitors (ASIs) such as abiraterone and enzalutamide (2–4). Despite this shift in therapeutic intervention, overall survival for CRPC patients has improved only marginally (3, 5, 6). Therefore, new mechanism-based studies are urgently needed to identify novel targets and strategies to treat CRPC patients who no longer respond to ASIs.

The Wnt/ $\beta$ -catenin signaling pathway is instrumental in orchestrating proper tissue development in embryos and tissue maintenance in adults (7). Increasing evidence has indicated that Wnt/ $\beta$ -catenin signaling is a major pathway associated with developing CRPC (8). Results from next-generation sequencing studies of CRPC specimens identified components of the Wnt/ $\beta$ -catenin signaling pathway with significant genomic alterations in CRPC (9). In low-androgen environments, AR and Wnt signaling may reinforce each other to elicit specific target genes that promote androgen-independent growth and progression. Given that  $\beta$ -catenin directly contributes to the activation of AR signaling (8), it is essential to define how upstream signaling events regulate the  $\beta$ -catenin pathway so that new approaches to treat non-ASI-responding CRPC can be developed.

Polo-like kinase 1 (Plk1), a critical regulator of many cell cycle-related events, is overexpressed in PCa, and high levels of Plk1 correlate with unfavorable patient outcomes (10). Therefore, Plk1 serves as a prognostic indicator for PCa patients and also serves as

a strong candidate target for the development of novel approaches to manage this disease (11). Of note, Plk1 is one of the top five upregulated pathways following castration (12). Several potent and selective ATP-competitive inhibitors of Plk1 have been shown to effectively inhibit tumor growth in *in vivo* studies (13, 14). Additionally, we recently reported that inhibition of Plk1 enhances the efficacy of ASIs in CRPC (15). In this study, we discovered that depletion or inhibition of Plk1 significantly reduces phosphorylated  $\beta$ -catenin levels and thus the stabilization of  $\beta$ -catenin protein in various prostate cancer cell lines. We also demonstrate that combinatorial inhibition of Plk1 and the Wnt/ $\beta$ -catenin pathway is a novel and therapeutically effective approach to treat CRPC in both cultured cells and LuCaP35CR tumors. Mechanistically, Plk1 inhibits  $\beta$ -catenin signaling through phosphorylation of axin2, the major antagonist of the Wnt/ $\beta$ -catenin pathway, leading to  $\beta$ -catenin degradation in human prostate cancer cells. Thus, inhibition of Plk1 activity results in the stabilization of  $\beta$ -catenin.

Received 26 August 2015 Returned for modification 15 September 2015

Accepted 25 September 2015

Accepted manuscript posted online 5 October 2015

Citation Li J, Karki A, Hodges KB, Ahmad N, Zoubeidi A, Strebhardt K, Ratliff TL, Konieczny SF, Liu X. 2015. Cotargeting Polo-like kinase 1 and the Wnt/ $\beta$ -catenin signaling pathway in castration-resistant prostate cancer. *Mol Cell Biol* 35:4185–4198. doi:10.1128/MCB.00825-15.

Address correspondence to Xiaoqi Liu, liu8@purdue.edu.

Copyright © 2015, American Society for Microbiology. All Rights Reserved.

## MATERIALS AND METHODS

**Cell culture and transfection.** PC3 cells were cultured in ATCC-formulated F-12K medium supplemented with 10% (vol/vol) fetal bovine serum (FBS) at 37°C in 5% CO<sub>2</sub>. LNCaP, C4-2, and 22Rv1 cells were cultured in RPMI 1640 medium with 10% FBS. Cells were transiently transfected with plasmid DNA with Lipofectamine 2000 transfection reagent from Invitrogen. Cells stably expressing wild-type axin2 (axin2-WT) or an axin2 mutant with an S-to-A change at position 311 (axin2-S311A) were obtained upon selection with 0.5 mg/ml G418 for 2 weeks.

**Reagents and plasmid DNA.** R1881 and nocodazole were purchased from Sigma. BI2536 and BIO [(2',3',5'-6-bromoindirubin-3'-oxime)] were obtained from Symansis and Tocris, respectively. IWR-1-endo (IWR1) and MDV3100 were purchased from Selleckchem. The human axin2 plasmid was kindly provided by Zhaoqiu Wu (University of Michigan). A site-directed mutagenesis kit (Agilent Technologies) was used to generate the specific mutation.

**Immunoblotting and immunoprecipitation.** Cell lysates were prepared in TBSN buffer (20 mM Tris, pH 8.0, 150 mM NaCl, 0.5% Nonidet P-40, 5 mM EGTA, 1.5 mM EDTA, 0.5 mM Na<sub>3</sub>VO<sub>4</sub>, 20 mM *p*-nitrophenyl phosphate) as described previously (16). For immunoprecipitation (IP), lysates were incubated with various antibodies in TBSN buffer at 4°C overnight, followed by 3 washes with TBSN buffer plus 500 mM NaCl and 3 additional washes with TBSN buffer plus 150 mM NaCl. For immunoblotting (IB), filters were incubated with specific antibodies at room temperature for 1 h, followed by an additional incubation with the secondary antibody for 30 min.

**Luciferase assay.** A T-cell factor/lymphoid enhancing factor (TCF/LEF) reporter kit was purchased from BPS Bioscience (catalog no. 60500), and luciferase assays were performed according to the manufacturer's instructions.

**Recombinant protein purification.** Coding sequences for various glutathione S-transferase (GST)-tagged human axin2 constructs (GenBank accession no. NM\_004655.3) were subcloned into pGEX-KG, and the constructs were expressed in *Escherichia coli* and purified. To purify Plk1 kinase, Hi5 insect cells were infected with baculovirus encoding GST-Plk1 and harvested 36 h after infection. Recombinant GST fusion proteins were affinity purified by incubation with glutathione-agarose beads from Sigma (catalog no. G4510), followed by extensive washes with STE buffer (10 mM Tris-HCl [pH 8.0], 1 mM EDTA, 150 mM NaCl) and elution with glutathione elution buffer (40 mM glutathione, 50 mM Tris-HCl, 10 mM dithiothreitol [DTT], 200 mM NaCl [pH 8.0]).

**Plk1 kinase assay.** *In vitro* kinase assays were performed with TBMD buffer (50 mM Tris [pH 7.5], 10 mM MgCl<sub>2</sub>, 5 mM dithiothreitol, 2 mM EGTA, 0.5 mM sodium vanadate, 20 mM *p*-nitrophenyl phosphate) supplemented with 125 μM ATP and 10 μCi of [<sup>32</sup>P]ATP at 30°C for 30 min in the presence of GST-axin2 proteins. After the reaction mixtures were resolved by SDS-PAGE, the gels were stained with Coomassie brilliant blue, dried, and subjected to autoradiography.

**Depletion and overexpression of Plk1.** HEK293T cells in 10-cm dishes were cotransfected with 4 μg of pHR'-CMV-ΔR 8.20vpr, 2 μg of pHR'-CMV-VSV-G, and 4 μg of pLKO.1-Plk1 (nucleotide 1424 relative to the starting codon) for depletion of Plk1 (17). Supernatants were collected every 12 h after 24 h posttransfection. Viruses were filtered through a 0.45-μm-pore-size filter, concentrated by spinning at 20,000 rpm for 2 h, resuspended in TNE buffer (50 mM Tris-HCl [pH 7.8], 130 mM NaCl, 1 mM EDTA), and rotated overnight at 4°C. Infections were carried out in the presence of 10 μg/ml of Polybrene and 10 mM HEPES, followed by selection with 1 μg/ml of puromycin for at least 36 h. Alternatively, PCa cells were cotransfected with pBS/U6-Plk1 (the targeting sequence of human Plk1 is GGGCGGCTTTGCCAAGTGCTT, corresponding to the coding region spanning positions 183 to 203 relative to the first nucleotide of the starting codon) and pBabe-puro at a ratio of 10:1 by using Lipofectamine 2000 reagents (18). Plasmid pBS/U6-Plk1-1st half (sense strand) was used as a control vector. This control vector produces RNA that cannot form a hairpin structure to generate interfering RNA. At 24 h

posttransfection, the medium was changed, and 2 μg/ml puromycin was added to select for transfection-positive cells. After 2 days of drug selection, floating cells were washed away, and the remaining attached cells were used for phenotype analysis. Adenovirus which overexpresses GFP-Plk1 was kindly provided by Kyung Lee (National Cancer Institute, MD).

**Antibodies.** The phospho-specific antibody against axin2-Ser311 was generated by Proteintech (Chicago, IL). Antibodies against Plk1 (catalog no. sc-17783), AR (catalog no. sc-7305), and green fluorescent protein (GFP) were purchased from Santa Cruz Biotechnology. Antibodies against Flag (catalog no. F-3165) and axin2 were purchased from Sigma and Abcam, respectively. Antibodies against β-catenin, Cdc20, prostate-specific antigen (PSA), and p-Ser9-glycogen synthase kinase 3β (p-Ser9-GSK3β) were purchased from Cell Signaling, whereas p-Tyr216-GSK3β antibody was purchased from BD Bioscience.

**Immunofluorescence staining.** Immunofluorescence (IF) staining was performed as described previously (15). Antibodies against β-catenin (catalog no. 610153; BD Transduction Laboratory) and/or AR (catalog no. 8956; cell signaling) were incubated for 1 h at room temperature, followed by incubation with secondary antibody and 4',6-diamidino-2-phenylindole (DAPI; Sigma) for 1 h.

**Combination index.** The combination index (CI) was calculated by using the equation combination index = (Am)<sub>50</sub>/(As)<sub>50</sub> + (Bm)<sub>50</sub>/(Bs)<sub>50</sub> (19), where (Am)<sub>50</sub> is the concentration of BI2536 necessary to achieve a 50% inhibitory effect in the combination with half of the concentration of the IWR1 50% inhibitory concentration (IC<sub>50</sub>), (As)<sub>50</sub> is the concentration of BI2536 that will produce the identical level of effect by itself, (Bm)<sub>50</sub> is the concentration of IWR1 that will produce a 50% inhibitory effect in the combination with half of the concentration of the BI2536 IC<sub>50</sub>, and (Bs)<sub>50</sub> is the concentration of IWR1 that will produce the same level of the effect by itself. Antagonism is indicated when the CI is >1; a CI equal to 1 indicates an additive effect, and a CI of <1 indicates synergy (20).

**PC3-derived mouse xenograft model.** All the animal experiments described in this study were approved by the Purdue University Animal Care and Use Committee. PC3 cells (1 × 10<sup>6</sup> cells per mouse) were inoculated into nude mice (Harlan Laboratories). Two weeks later, animals were randomized into treatment and control groups of 4 mice each. BI2536 was injected into the tail vein twice weekly. The IWR1 suspension was prepared in coin oil and administered to mice via oral gavage twice weekly. Tumor volumes, calculated from the formula  $V = L \times W^2/2$  (where *V* is volume [cubic millimeters], *L* is length [millimeters], and *W* is width [millimeters]).

**LuCaP35CR xenograft model.** Mice carrying LuCaP35CR tumors were obtained from Robert Vessella at the University of Washington. Tumors were amplified and then implanted into precastrated nude mice. After enough tumors were amplified, tumors were harvested and cut into ~20- to 30-mm<sup>3</sup> pieces before being implanted into 16 precastrated nude mice. When tumors reached 200 to 300 mm<sup>3</sup>, mice were randomly separated into 4 groups for different treatments, as described above.

**Histology and immunohistochemistry.** Xenograft tumors were fixed in 10% neutral buffered formalin, paraffin embedded, sectioned to 5 μm, and stained by using conventional hematoxylin-and-eosin (H&E) staining. Human prostate tissues were kindly provided by Liang Cheng (Indiana University, IN) and also purchased from U.S. Biomax. Immunohistochemistry (IHC) and immunofluorescent chemistry (IFC) staining were accomplished with the Elite Vectastain ABC kit.

**Statistical analysis.** The statistical significance of the results was analyzed by using an unpaired Student *t* test (StatView I; Abacus Concepts Inc., Berkeley, CA), except for the data in Fig. 6M, which were analyzed by a χ<sup>2</sup> test. A *P* value of <0.05 indicates statistical significance.

## RESULTS

**Inhibition of Plk1 activates Wnt/β-catenin signaling in human prostate cancer cells.** Plk1 is overexpressed in PCa cells, is involved in PCa tumorigenesis and progression (10), and is one of

the top upregulated pathways following castration in PCa xenograft models (12). The Wnt/ $\beta$ -catenin pathway is also a major pathway activated in CRPC (9). However, whether there is cross talk between Plk1 and Wnt/ $\beta$ -catenin signaling in the context of CRPC is not known. Accordingly, we asked if modulation of Plk1 could significantly alter the status of the  $\beta$ -catenin pathway.

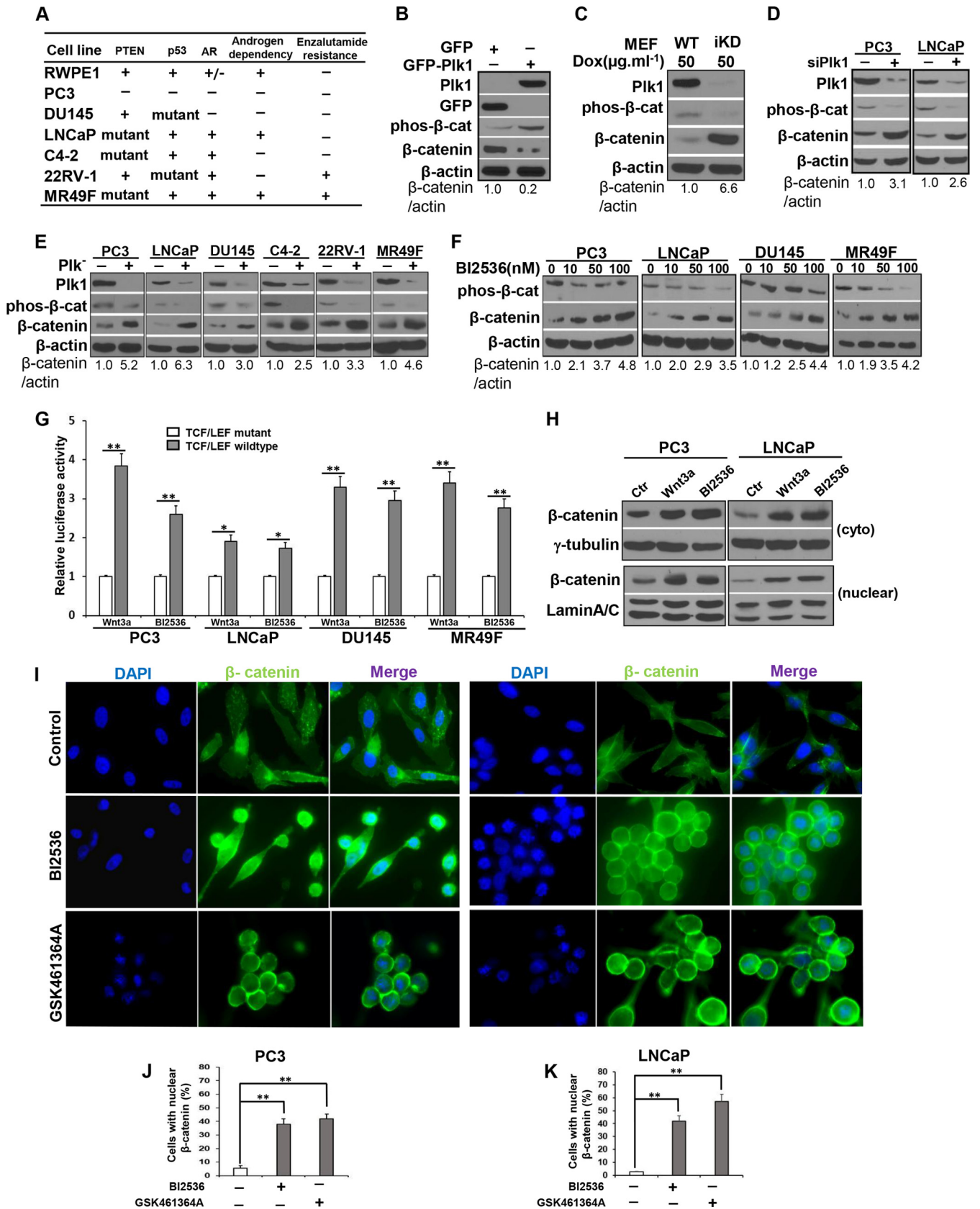
Considering that depletion of Plk1 leads to mitotic arrest in cancer cells but not in nontransformed cells (17), we first employed an adenovirus-based approach to overexpress GFP-Plk1 in the RWPE1 cell line, a nontransformed and immortal human prostate cell line (Fig. 1A) (21). Overexpression of Plk1 in normal RWPE1 cells increased the level of phosphorylated  $\beta$ -catenin and promoted its degradation (Fig. 1B), suggesting that Plk1 might function as a negative regulator of the Wnt/ $\beta$ -catenin pathway. In support, Plk1 knockdown in mouse embryonic fibroblasts (MEFs) decreased the level of phosphorylated  $\beta$ -catenin and promoted its stabilization (Fig. 1C) (22). To examine this further, we investigated the Plk1/ $\beta$ -catenin connection in a panel of PCa cell lines with diverse genetic backgrounds (Fig. 1A). While PC3 and DU145 cells are AR-null cells, the LNCaP cell line, its derivative cell lines (C4-2 and MR49F), and 22RV-1 cells express AR. Furthermore, LNCaP cells are androgen dependent, but C4-2 and 22RV-1 cells are considered CRPC cells, as their growth is androgen independent. Finally, MR49F cells are derived from LNCaP cells but are enzalutamide resistant (23). Vector-based small interfering RNA (siRNA) technology (the targeting sequence of human Plk1 is the coding region spanning positions 183 to 203 relative to the starting codon) (Fig. 1D) (18) and a lentivirus-based RNA interference (RNAi) system (the targeting sequence of human Plk1 is the coding region spanning positions 1424 to 1444 relative to the starting codon) (Fig. 1E) (17) were used to deplete Plk1 in PCa cell lines. Interestingly, both depletion of Plk1 (Fig. 1D and E) and inhibition of Plk1 activity with BI2536 (Fig. 1F) resulted in reduced levels of phosphorylated  $\beta$ -catenin and stabilization of  $\beta$ -catenin in PCa cells with diverse genetic backgrounds. These results suggest that Plk1 inhibition-associated activation of the Wnt/ $\beta$ -catenin signaling pathway is a general phenomenon in PCa. In agreement, using a TCF/LEF reporter assay, we found that inhibition of Plk1 by BI2536 generated increased transcriptional activity of the  $\beta$ -catenin pathway (Fig. 1G). Since active  $\beta$ -catenin shuttles into the nucleus to function as a transcription factor, we also analyzed its subcellular localization by cell fractionation upon inhibition of Plk1 activity. We found that inhibition of Plk1 by BI2536 led to the accumulation of total  $\beta$ -catenin and enhanced both cytosolic and nuclear  $\beta$ -catenin in PC3 and LNCaP cells (Fig. 1H). Finally, we performed anti- $\beta$ -catenin immunofluorescence (IF) analysis and further confirmed the enhanced levels of cytosolic and nuclear  $\beta$ -catenin upon treatment with both BI2536 and GSK461364A, another Plk1 inhibitor currently in clinical trials (24, 25) (Fig. 1I to K). Altogether, these results demonstrate that Plk1 is a negative regulator of the Wnt/ $\beta$ -catenin pathway and that Plk1 inhibition induces  $\beta$ -catenin stabilization in human PCa cells, including CRPC and enzalutamide-resistant PCa cells.

**Inhibition of Wnt/ $\beta$ -catenin signaling enhances the efficacy of BI2536 antineoplastic activity in PC3-derived xenograft tumors.** Because inhibition of Plk1 activates Wnt/ $\beta$ -catenin signaling in cells representing various stages of PCa, we asked whether BI2536 and the Wnt signaling inhibitor IWR1-1-endo (IWR1) (Fig. 2A) act synergistically to inhibit the growth of PCa. First, PC3 cells

were treated with BI2536, IWR1, or BI2536 in combination with IWR1 and harvested for analysis of cleaved poly(ADP-ribose) polymerase (PARP), a marker of apoptosis. As predicted, the combination of BI2536 and IWR1 led to significantly increased cellular apoptotic responses compared to those with BI2536 or IWR1 alone (Fig. 2B). Next, we performed fluorescence-activated cell sorter (FACS) analysis to monitor any cell cycle defect upon drug treatment. As indicated, the presence of IWR1 potentiated BI2536-associated cell death in PC3 cells (Fig. 2C). In agreement, treatment of PC3 cells with the combination of BI2536 and IWR1 showed a much stronger inhibitory effect on colony formation than with BI2536 or IWR1 alone (Fig. 2D and E). Measurements of  $IC_{50}$ s also revealed an  $IC_{50}$  of 12  $\mu$ mol/liter for BI2536-treated PC3 cells (Fig. 2F). However, the  $IC_{50}$  of BI2536 was reduced to 2  $\mu$ mol/liter when cells were treated in combination with 30  $\mu$ mol/liter IWR1. The combination index of the two drugs was calculated to be 0.233 ( $<0.3$ ), suggesting a strong synergistic effect between BI2536 and IWR1.

To better assess this synergistic activity, we next tested the effect of combination treatment on a PC3-derived xenograft mouse model. As shown in Fig. 2G, the combination of BI2536 and IWR1 led to a significantly greater tumor-inhibitory effect than did monotherapy with either BI2536 or IWR1. Histological analyses of these tumors under different treatment conditions revealed that tumors from the control group exhibited sheets of malignant cells with marked nuclear pleomorphism, numerous mitotic figures (Fig. 2H), and high Ki67 levels (Fig. 2H and I). These histopathological features are similar to those of high-grade prostatic adenocarcinoma *in vivo*, which is typically associated with poor clinical outcomes. IWR1-treated tumors showed an invasive growth pattern with infiltrative margins in the skeletal muscle. However, treatment with BI2536 altered the tumor growth pattern so that there was a significant decrease in skeletal muscle invasion (Fig. 2H). Finally, histological sections of the small residual tissue nodule that remained following combined BI2536 and IWR1 treatment predominantly revealed skeletal muscle devoid of malignant cells, suggesting that the combination of BI2536 and IWR1 is a more effective approach to killing PCa cells than monotherapy with BI2536. These results are consistent with our observations with the cell-based study, providing additional evidence of a strong synergistic effect between BI2536 and IWR1 *in vitro* and *in vivo*.

**Combination therapy with BI2536 and IWR1 blocks growth of CRPC.** Because CRPC is an extremely heterogeneous disease and is generally driven by AR, although only a small percentage of cases are AR negative, it is important to use a different model to confirm the synergistic effect between BI2536 and the Wnt signaling inhibitor. Accordingly, we moved on to use the castration-resistant LuCaP35CR xenograft model, which is AR positive (26, 27). As predicted, monotherapies with BI2536 or IWR1 did not significantly affect castration-resistant tumor growth (Fig. 3A) and serum PSA levels (Fig. 4A). In contrast, combination therapy using BI2536 and IWR1 not only completely blocked tumor growth but also induced regression of tumors at the end of the study (Fig. 3B). Histological analyses of these CRPC tumors showed that tumors from the control group exhibited high-grade prostatic adenocarcinoma characterized by large nuclei, clear chromatin, prominent nucleoli, and numerous mitotic figures (Fig. 3C). Higher magnification revealed a delicate vascular network throughout the tumor. Tumors from IWR1-treated mice



showed similar cytomorphological features, although the vascular network was more prominent, and the tumor had a more nested appearance. BI2536-treated tumors showed apoptotic bodies and morphological changes of necrosis, including shrinkage of tumor nests, nuclear pyknosis, and karyorrhexis with an inflammatory cell infiltrate. Remarkably, the tumors treated with BI2536 plus IWR1 showed marked apoptotic bodies with a condensed cytoplasm and pyknotic nuclei (Fig. 3C). Immunostaining for Ki67 and cleaved caspase 3 also confirmed that tumors from combination therapy had a significant reduction in overall proliferation and a significant increase in apoptosis. (Fig. 3C to E). Similarly, AR localization was affected. Nuclear AR colocalized with  $\beta$ -catenin in BI2536-treated LuCaP35CR tumors, but the intensity of AR and its colocalization with  $\beta$ -catenin became significantly reduced in tumors treated with BI2536 plus IWR1 (Fig. 4B and C). Because MR49F cells are enzalutamide resistant, it is of clinical significance to ask whether treatment with BI2536 plus IWR1 affects the cellular response to enzalutamide (previously MDV3100). First, as predicted, BI2536 treatment led to increased levels of both cytosolic and nuclear  $\beta$ -catenin in MR49F cells (Fig. 4D). Second, treatment with BI2536 plus IWR1 dramatically inhibited AR intensity and nuclear AR levels (Fig. 4E and F). Finally, inhibition of Plk1 activity potentiated enzalutamide-associated cell death, and cotargeting of Plk1 and Wnt/ $\beta$ -catenin signaling can further sensitize MR49F cells to enzalutamide. This was indicated by an almost complete disappearance of AR protein and a substantial increase in the level of cleaved PARP (Fig. 4G). Considering that enzalutamide is a major drug used in clinical situations for advanced-stage PCa, our data are particularly significant, strongly suggesting that cotargeting the Plk1 and Wnt/ $\beta$ -catenin pathway could be an effective strategy to treat ASI-resistant CRPC. In summary, these experiments support the notion that inhibition of Plk1 and inhibition of Wnt/ $\beta$ -catenin signaling act synergistically in CRPC, providing a novel and promising therapeutic option to treat CRPC patients.

**Plk1 phosphorylates axin2.** To uncover the mechanism behind the strong synergistic effect between Plk1 and Wnt inhibitors in blocking human prostate tumor growth, we aimed to identify how Plk1 inhibition enhances cytosolic and nuclear  $\beta$ -catenin levels, leading to elevated Wnt/ $\beta$ -catenin signaling. In search of Plk1-interacting proteins using mass spectrometry, we identified axin2, a negative regulator of the Wnt/ $\beta$ -catenin pathway, as a potential Plk1 substrate (28). Considering that Plk1 is a mitotic kinase, we first asked whether the expression of axin2 is cell cycle regulated.

Accordingly, PC3 or LNCaP cells were synchronized with a double-thymidine block at the G<sub>1</sub>/S boundary and released for different times. As shown in Fig. 5A and C, expression of axin2 started in late S phase, accumulated in G<sub>2</sub> phase, and reached a peak in mitosis in both PC3 and LNCaP cells, precisely matching the Plk1 expression pattern. Confirmatory results were obtained when cells were arrested at the G<sub>2</sub>/M phase by nocodazole treatment (Fig. 5B and D), revealing that expression of axin2, similarly to Plk1, is regulated in a cell cycle-dependent manner in human PCa cells. Next, coimmunoprecipitation experiments showed that endogenous Plk1 binds to endogenous axin2 (Fig. 5E). These results suggest that both Plk1 and axin2 are upregulated at G<sub>2</sub>/M phase and that Plk1 forms a stable complex with axin2 in human PCa cells. We then sought to determine if axin2 functions as a direct substrate for Plk1. Using recombinant GST-axin2 fragments, we next discovered that the axin2 region from amino acids (aa) 301 to 577 was phosphorylated by Plk1 (Fig. 5F). To more precisely map the phosphorylation site(s), we mutated every serine/threonine within the region spanning aa 301 to 577 to alanine and eventually identified that Plk1 directly phosphorylates axin2 at S311 (Fig. 5G). Plk1 phosphorylation of axin2 at S311 was confirmed by IB using a phospho-specific antibody (pS311-axin2) (Fig. 5H). Having established the specificity of the pS311-axin2 antibody, we asked whether S311 of axin2 is similarly phosphorylated by Plk1 in human PCa cells. As shown in Fig. 5I, RNAi-mediated Plk1 depletion completely abolished the phosphorylation of pS311 in nocodazole-treated PC3 cells, suggesting that Plk1 is indeed the major kinase responsible for axin2-S311 phosphorylation *in vivo*. Moreover, the level of S311 phosphorylation of ectopically expressed axin2 was inhibited by BI2536 in a dose-dependent manner (Fig. 5J), further supporting the notion that phosphorylation of axin2-S311 is dependent on Plk1-associated kinase activity. Furthermore, anti-pS311-axin2 detected phosphorylated axin2 in lysates from mitotic cells, but the level of S311 phosphorylation was significantly lower for BI2536-treated cells, again arguing that endogenous axin2 is phosphorylated at S311 by endogenous Plk1 (Fig. 5K). We also asked whether S311 phosphorylation of axin2 is cell cycle regulated by examining PC3 and LNCaP cells released from a nocodazole block. As shown in Fig. 5L and M, the pS311-axin2 epitope was detected in nocodazole-blocked cells, and its expression gradually decreased as cells exited mitosis, matching the pattern of Plk1 expression. Finally, we acknowledge that the *in vitro* kinase assay shows that the first axin2 fragment (aa 1 to 300) exhibits a weak phosphorylation signal (Fig. 5F), possibly indicat-

**FIG 1** Plk1 negatively regulates the Wnt/ $\beta$ -catenin pathway in human prostate cancer cells. (A) Genetic backgrounds of prostate cell lines used in this study. (B) Overexpression of Plk1 inhibits  $\beta$ -catenin signaling in RWPE1 cells. RWPE1 cells were infected with adenovirus expressing GFP or GFP-Plk1 for 48 h and harvested for immunoblotting (IB) with the antibodies indicated. (C) Knockdown of Plk1 activates Wnt/ $\beta$ -catenin signaling in MEFs from Plk1-inducible knockdown (iKD) mice. MEFs were harvested for IB after 96 h of treatment with doxycycline (Dox) ( $50 \mu\text{g} \cdot \text{ml}^{-1}$ ). (D) Vector-based siRNA targeting Plk1. PC3 or LNCaP cells were cotransfected with pBS/U6-Plk1 or the control vector and pBabe-puro at a ratio of 10:1. At 24 h posttransfection, the medium was changed, and  $2 \mu\text{g}/\text{ml}$  puromycin was added to select for transfection-positive cells. After a 2-day selection with puromycin, floating cells were washed away, and the remaining attached cells were harvested for IB. (E) Depletion of Plk1 stabilizes  $\beta$ -catenin in various human prostate cancer cells. PC3, LNCaP, DU145, C4-2, 22RV-1, or MR49F cells were infected with lentivirus for 36 h to deplete Plk1 and harvested for IB. (F) Inhibition of Plk1 leads to activation of Wnt/ $\beta$ -catenin signaling. PCa cells were treated with the indicated concentrations of BI2536 for 16 h. (G) Cells were cotransfected with the TCF/LEF luciferase reporter vector or a noninducible TCF/LEF mutant luciferase vector and a constitutively expressing *Renilla* luciferase vector (internal control), followed by treatment with Wnt3a or BI2536. Luciferase activity is reported as relative activity (luciferase/*Renilla*) and represented as means  $\pm$  standard deviations of data from 3 replicates. Wnt3a (as a positive control) is an established agonist of the Wnt/ $\beta$ -catenin pathway. \*,  $P < 0.05$ ; \*\*,  $P < 0.01$ . (H) Plk1 inhibition enhances the levels of cytosolic and nuclear  $\beta$ -catenin. PC3 and LNCaP cells were treated with BI2536 or Wnt3a, followed by subcellular fractionation. (I to K) Representative confocal microscopy images of enhanced levels of cytosolic and nuclear  $\beta$ -catenin in PC3 and LNCaP cells treated with BI2536 or GSK46136A for 16 h (I) and quantified (J and K) (means  $\pm$  standard errors of the means;  $n = 3$  independent experiments, where 500 cells were counted in each group). \*\*,  $P < 0.01$ . All Western blots are representative of data from three or more experiments.

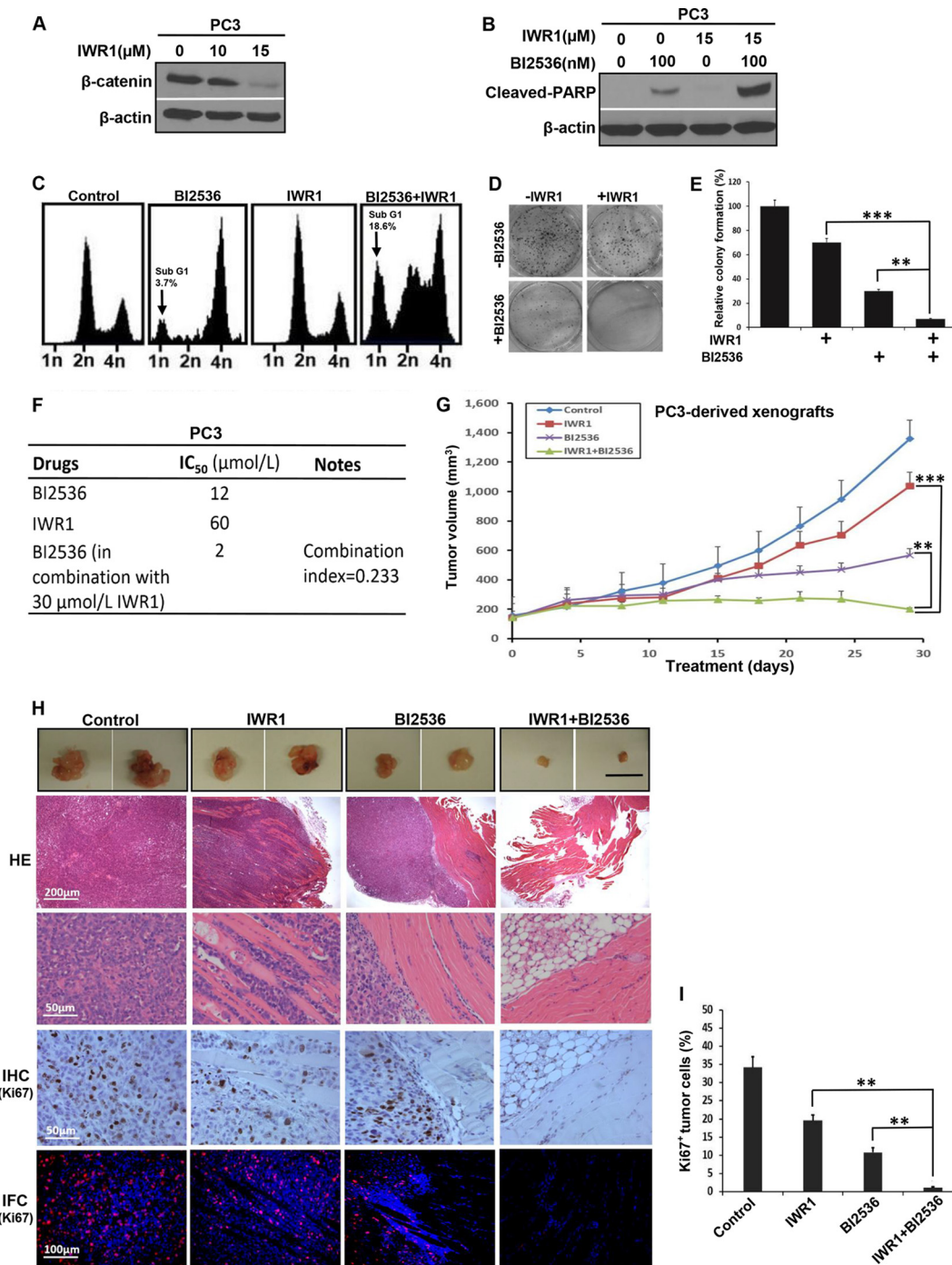


**FIG 2** BI2536 and IWR1 synergistically inhibit growth of PC3 cell-derived xenograft tumors. (A) PC3 cells were treated with increasing concentrations of IWR1 for 24 h and harvested. (B) PC3 cells were treated with BI2536, IWR1, or both for 24 h, followed by IB. (C) PC3 cells were treated with BI2536, IWR1, or both for 4 days. Harvested cells were subjected to FACS analysis. (D) PC3 cells ( $0.5 \times 10^3$ ) were plated into 6-well plates for 24 h and then treated with BI2536, IWR1, or both drugs. After changing to fresh medium containing the drug(s) every 3 days for 2 weeks, cells were paraformaldehyde fixed, and colony formation was monitored by crystal violet staining. Data shown are representative of data from 3 repeats. (E) Quantification of colonies in panel D. The numbers of colonies were quantified by using ImageJ software (means  $\pm$  standard deviations;  $n = 3$  independent experiments). \*\*,  $P < 0.01$ ; \*\*\*,  $P < 0.001$ . (F) Combination indexes of BI2536 and IWR1 in PC3 cells. (G) Tumor growth curves of PC3-derived mouse xenografts. Nude mice were inoculated with PC3 cells ( $1 \times 10^6$ ) for 2 weeks and intravenously injected with BI2536 (12 mg/kg of body weight), IWR1 (50 mg/kg), or a combination of both drugs by oral gavage. The sizes of the tumors in each group were measured every 3 days (means  $\pm$  standard errors of the means;  $n = 4$  mice from each experimental group). \*\*,  $P < 0.01$  compared with the BI2536-treated group on day 29; \*\*\*,  $P < 0.001$  compared with the IWR1-treated group on day 29. (H) Representative images of H&E and IHC or IFC staining for Ki67 on formaldehyde-fixed, paraffin-embedded, PC3-derived tumor sections. (I) Microscopic quantification of Ki67 signals as percentages of Ki67-positive cells compared to total numbers of cells. Multiple tumor sections were calculated (means  $\pm$  standard errors of the means;  $n = 4$ ). \*\*,  $P < 0.01$ . Western blots in panels A and B are representative of results from three or more experiments.

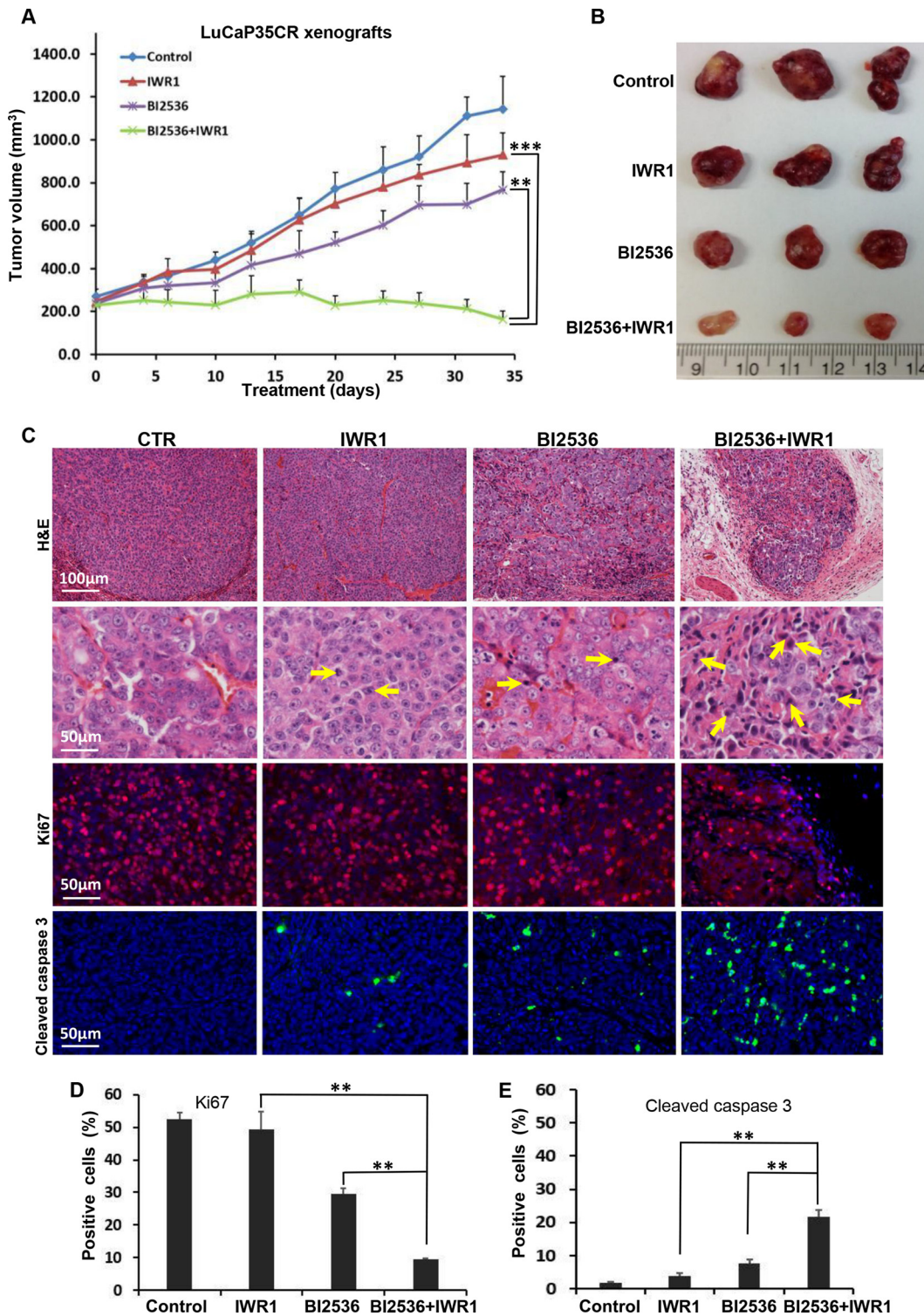


**FIG 3** BI2536 and IWR1 inhibit LuCaP35CR xenografts synergistically. LuCaP35CR tumors were inoculated into nude mice, which had been castrated 2 weeks earlier. After waiting for several weeks for tumors to reach a size of 200 to 300 mm<sup>3</sup>, mice were intravenously injected twice per week with BI2536 (15 mg/kg), IWR1 (60 mg/kg), or both by oral gavage and monitored for an additional 34 days. (A) Tumor growth curves (means  $\pm$  standard errors of the means;  $n = 4$  mice from each experimental group). \*\*,  $P < 0.01$  compared with the BI2536-treated group on day 34; \*\*\*,  $P < 0.001$  compared with the IWR1-treated group on day 34. (B) Images of tumors at the end of the study. (C) Representative images of H&E and IFC staining for Ki67 and cleaved caspase 3 on formaldehyde-fixed, paraffin-embedded LuCaP35CR tumor sections from the different treatment groups in panel A. (D and E) Microscopic quantification of Ki67 or cleaved caspase 3 as a percentage of Ki67- or cleaved caspase 3-positive cells compared to the total number of cells. Values for multiple tumor sections were calculated (means  $\pm$  standard errors of the means;  $n = 4$ ). \*\*,  $P < 0.01$ .

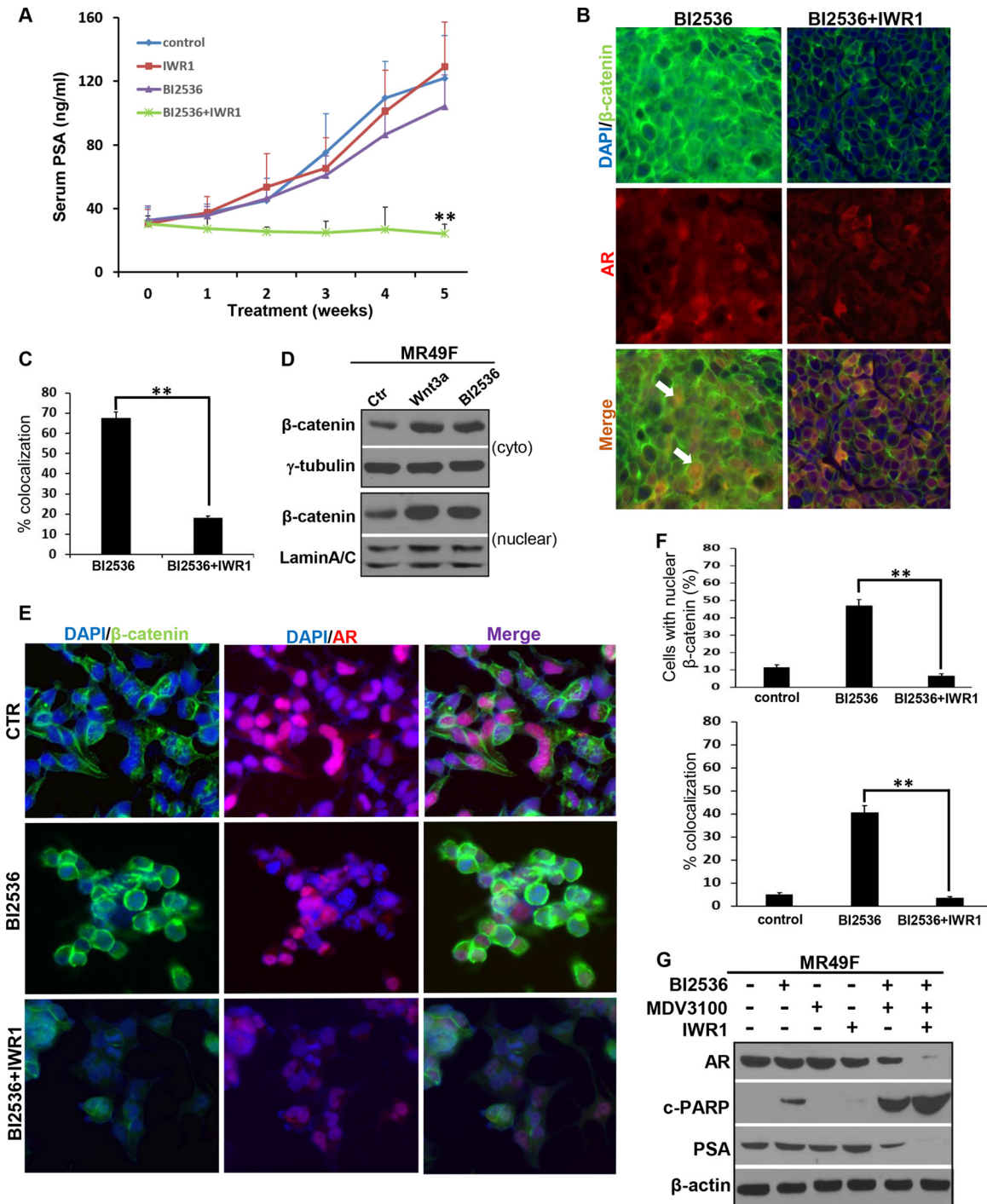


**FIG 4** Combinational inhibition of Plk1 and Wnt/β-catenin signaling decreases AR intensity and its nuclear localization. (A) Inhibition of PSA levels by BI2536 and IWR1. Blood was collected once a week from LuCaP35CR tumor-bearing mice, and serum PSA levels were measured by using a PSA enzyme-linked immunosorbent assay kit. Data shown are means ± standard errors of the means. \*\*,  $P < 0.01$  compared with the BI2536-treated group. (B) Colocalization of AR and β-catenin in LuCaP35CR tumors after treatment with BI2536 alone but not in tumors treated with BI2536 plus IWR1. Sections of LuCaP35CR xenografts, as described in the Fig. 3 legend, were stained with antibodies against β-catenin together with antibodies against AR. Arrows indicate cells with nuclear colocalization of AR and β-catenin. (C) Graph showing percentages of colocalization of β-catenin and AR from panel B. Results were calculated for multiple tumor sections. (D) Inhibition of Plk1 enhances the levels of cytosolic and nuclear β-catenin in MR49F cells. Cells were treated with BI2536 or Wnt3a (as a positive control), followed by subcellular fractionation. (E) Combined inhibition of Plk1 and β-catenin decreases AR nuclear localization and intensity in MR49F cells. Cells were treated with BI2536 (20 nM) or BI2536 plus IWR1 (15 μM) for 24 h and costained with antibodies against β-catenin and AR. Shown are representative images from 3 experiments. (F) Quantification of cells with nuclear β-catenin and percentage of colocalization of β-catenin and AR from panel E. (G) Inhibition of Wnt/β-catenin signaling further potentiates cell death associated with treatment with BI2536 plus enzalutamide. MR49F cells were treated with BI2536 (20 nM), IWR1 (15 μM), enzalutamide (10 μM), or a combination of the 3 drugs for 24 h and harvested. Data in panels C and F are expressed as means ± standard errors of the means (error bars). \*\*,  $P < 0.01$ . Western blots in panels D and G are representative of results from three or more experiments.

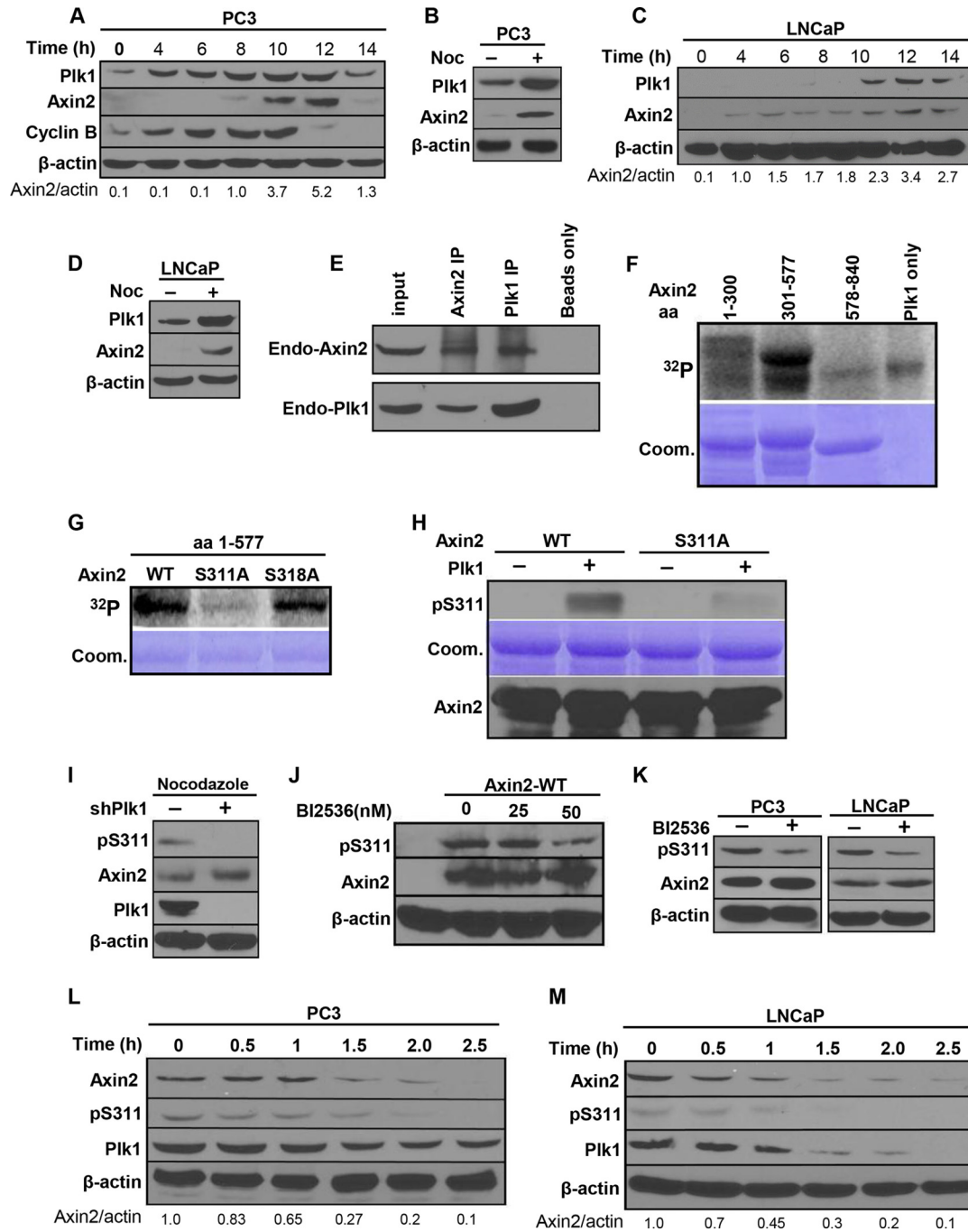


**FIG 5** Plk1 phosphorylates axin2 at Ser311. (A to D) Cell cycle-regulated expression of axin2 and Plk1. (A and C) PC3 (A) and LNCaP (C) cells were synchronized with a double-thymidine block (DTB) (16-h thymidine block, 8 h of release, and a second thymidine treatment for 16 h), released for different times, and harvested for IB. (B and D) PC3 (B) and LNCaP (D) cells were treated with or without nocodazole for 12 h and harvested. (E) Axin2 binds to Plk1. PC3 cells were treated with nocodazole and harvested for IP with antibodies against Plk1 or axin2, followed by IB. (F) Plk1 targets N-terminal axin2. Purified Plk1 was incubated with purified GST-axin2 regions (aa 1 to 300, aa 301 to 577, and aa 578 to 840) in the presence of [ $\gamma$ - $^{32}$ P]ATP. The reaction mixtures were resolved by SDS-PAGE, stained with Coomassie brilliant blue (Coom.), and detected by autoradiography. (G) Plk1 phosphorylates axin2 at Ser311 *in vitro*. Purified Plk1 was incubated with different recombinant axin2 regions spanning aa 1 to 577 (WT, S311A mutant, or S318A mutant) and analyzed. (H) pSer311-axin2 antibody specifically recognizes the phosphorylated form of axin2. Recombinant axin2 proteins (WT or S311A) were incubated with or without purified Plk1 in the presence of unlabeled ATP and immunoblotted with the pSer311-axin2 antibody. (I) Axin2-Ser311 is phosphorylated *in vivo* in a Plk1 activity-dependent manner. PC3 cells were cotransfected with pBS/U6-Plk1 and pBabe-puro at a ratio of 8:1. After a 2-day selection of transfection-positive cells with puromycin, attached cells were treated with nocodazole and harvested for IB. shPlk1, short hairpin RNA against Plk1. (J) Inhibition of Plk1 activity downregulates the phosphorylation level of axin2 at S311. HEK293T cells were transfected with Flag-axin2 and treated with BI2536 for 8 h in the presence of nocodazole. (K) Inhibition of Plk1 activity downregulates the phosphorylation level of endogenous axin2 at S311. PC3 or LNCaP cells were treated with 50 nM BI2536 for 8 h in the presence of nocodazole. (L and M) Cell cycle-dependent phosphorylation of axin2-S311. After treatment with nocodazole, PC3 (L) or LNCaP (M) cells were collected with mitotic shake-off, released for different times, and harvested. All data shown are representative of results from three or more experiments.

ing an additional minor phosphorylation site. However, considering that the region spanning aa 301 to 577 is clearly phosphorylated to higher levels than the weakly phosphorylated fragment spanning aa 1 to 300, we focused on the functional analysis of S311 for the rest of the study. Collectively, we conclude that Plk1 phosphorylates axin2 both *in vitro* and *in vivo*.

**Plk1 phosphorylation of axin2 is involved in  $\beta$ -catenin degradation in human PCa cells.**  $\beta$ -Catenin, the major effector of the Wnt signaling pathway, is essential for many developmental processes and has been implicated in tumorigenesis in PCa (8). It is well established that axin2 serves as a negative regulator of the Wnt/ $\beta$ -catenin pathway by promoting the phosphorylation, and subsequent degradation, of  $\beta$ -catenin (29). To test whether Plk1 phosphorylation of axin2 affects the modulation of  $\beta$ -catenin in human PCa cells, we ectopically expressed different axin2 constructs (WT and S311A) in PC3 and LNCaP cells. As expected, overexpression of axin2-WT promoted the degradation of  $\beta$ -catenin. In contrast, introduction of the S311A mutation antagonized axin2 expression-induced degradation of  $\beta$ -catenin (Fig. 6A and B), suggesting that Plk1 phosphorylation of axin2 enhances its function as a negative regulator of  $\beta$ -catenin signaling.

$\beta$ -Catenin interacts with AR and enhances AR-mediated transactivation activity in PCa cells (30, 31). Therefore, we next asked whether Plk1 phosphorylation of axin2 also affects AR-mediated transactivation activity. In comparison to LNCaP cells expressing axin2-WT, LNCaP cells expressing axin2-S311A exhibited much higher levels of  $\beta$ -catenin and prostate-specific antigen (PSA), a major downstream target of AR (Fig. 6B). Treatment of LNCaP cells with androgen R1881 increased the basal level of PSA, but cells expressing axin2-S311A clearly had a much higher level of PSA (Fig. 6C). To further confirm that Plk1-associated kinase activity toward axin2-S311A regulates  $\beta$ -catenin stability and PSA levels, we repeated these experiments in the presence of BI2536. As shown in Fig. 6D and E, BI2536 treatment abolished axin2-WT overexpression-induced degradation of  $\beta$ -catenin and PSA, restoring the levels of  $\beta$ -catenin and PSA to those observed in cells expressing axin2-S311A. Collectively, these data support the notion that Plk1 phosphorylation of axin2 facilitates degradation of  $\beta$ -catenin.

Previous studies have shown that enhancing the level of cytosolic  $\beta$ -catenin using purified Wnt3a protein can promote cell growth in PC3 and LNCaP cells (32). Because cells expressing different forms of axin2 (WT and S311A) showed different levels of  $\beta$ -catenin, we tested if Plk1 phosphorylation of axin2 affects cell proliferation. Cells expressing axin2-S311A exhibited a greater colony formation ability (Fig. 6F and G) than did cells expressing axin2-WT. Finally, we directly compared the tumor-forming abilities of PC3 cells stably expressing different forms of axin2 (WT or S311A). As indicated in Fig. 6H and I, the volumes of tumors expressing axin2-WT were significantly reduced compared to those of tumors expressing axin2-S311A. IHC staining indicated that tumors expressing axin2-S311A had a higher proliferation rate and a higher level of  $\beta$ -catenin expression (Fig. 6J and K). Furthermore, we conducted IHC staining of Plk1, axin2, and  $\beta$ -catenin in both normal human prostate tissue and malignant prostate tumors and found that high expression levels of Plk1 and  $\beta$ -catenin correlate with a low expression level of axin2 in malignant tumors (Fig. 6L and M). Taken together, these data suggest that Plk1 phosphorylation of axin2 is a major mechanism that facilitates the degradation of  $\beta$ -catenin in PCa cells. We conclude that dysregulation

of Plk1-associated axin2 phosphorylation results in activation of the Wnt/ $\beta$ -catenin pathway in PCa, which is linked with higher grades of PCa tumors.

**Plk1 phosphorylation of axin2 enhances binding between GSK3 $\beta$  and  $\beta$ -catenin.** Next, we aimed to further dissect the underlying mechanism for Plk1 phosphorylation of axin2 mediating the degradation of  $\beta$ -catenin. Considering that GSK3 $\beta$  is a negative regulator of both  $\beta$ -catenin and AR-mediated transcription (33–35). We hypothesized that Plk1 phosphorylation of axin2 mediates degradation of  $\beta$ -catenin through GSK3 $\beta$ . To test this directly, PC3 cells were transfected with different forms of axin2 (WT and S311A) and harvested for IP with  $\beta$ -catenin antibodies, followed by IB for axin2, GSK3 $\beta$ , and  $\beta$ -catenin. As indicated, binding between GSK3 $\beta$  and  $\beta$ -catenin was remarkably decreased in cells overexpressing axin2-S311A compared to cells expressing axin2-WT (Fig. 7A), suggesting that Plk1 phosphorylation of axin2 is critical for binding between GSK3 $\beta$  and  $\beta$ -catenin, an essential step for the subsequent degradation of  $\beta$ -catenin.

Because GSK3 $\beta$ -dependent phosphorylation of  $\beta$ -catenin leads to its degradation, inhibition of GSK3 $\beta$  causes stabilization of  $\beta$ -catenin (Fig. 7B). However, because the binding of GSK3 $\beta$  and  $\beta$ -catenin is inhibited in cells expressing axin2-S311A, we predict that the level of  $\beta$ -catenin will be constitutively higher under these conditions. Indeed, this was verified in both PC3 (Fig. 7C) and LNCaP (Fig. 7D) cells, further supporting a relatively lower level of interaction between GSK3 $\beta$  and  $\beta$ -catenin upon axin2-S311A expression.

**Plk1 phosphorylation of axin2 leads to increased resistance to Cdc20-mediated degradation.** We aimed to search for additional mechanisms to understand how Plk1 phosphorylation of axin2 is involved in degradation of  $\beta$ -catenin. Cdc20 is a positive regulator of the anaphase-promoting complex (APC), an E3 ubiquitin ligase that controls the degradation of many mitotic proteins. It has been reported that axin2 protein stability is regulated by Cdc20 (36). We thus asked whether Plk1 phosphorylation of axin2 also regulates Cdc20-mediated degradation by coexpressing HA-Cdc20 with different axin2 constructs (WT and S311A). As indicated, axin2-WT appears to be more resistant to Cdc20 expression-induced degradation than axin2-S311A in both PC3 (Fig. 7E) and LNCaP (Fig. 7F) cells, suggesting that Plk1 phosphorylation of axin2 also antagonizes Cdc20-mediated degradation. This is in agreement with data from a previous study showing that Cdc20-resistant axin2 inhibits the Wnt/ $\beta$ -catenin pathway and attenuates colony formation (36). Such an observation is also consistent with our above-described data showing that cells expressing axin2-WT exhibit significantly reduced colony formation ability compared to that of cells expressing axin2-S311A (Fig. 6F).

## DISCUSSION

**Plk1 in CRPC treatment.** ASI-based target therapy is one major approach to treat patients with CRPC. However, resistance to powerful antiandrogens such as abiraterone or enzalutamide occurs rapidly (3, 6). Therefore, CRPC remains an incurable disease, reflecting the urgency to develop new approaches to enhance the efficacy of ASIs. In this regard, a number of experimental facts support the notion that Plk1 could be an important target whose inhibition can overcome therapy resistance in CRPC. First, castration, the major approach to treat late-stage PCa, activates many downstream signaling pathways, in which Plk1 is one of the top five upregulated

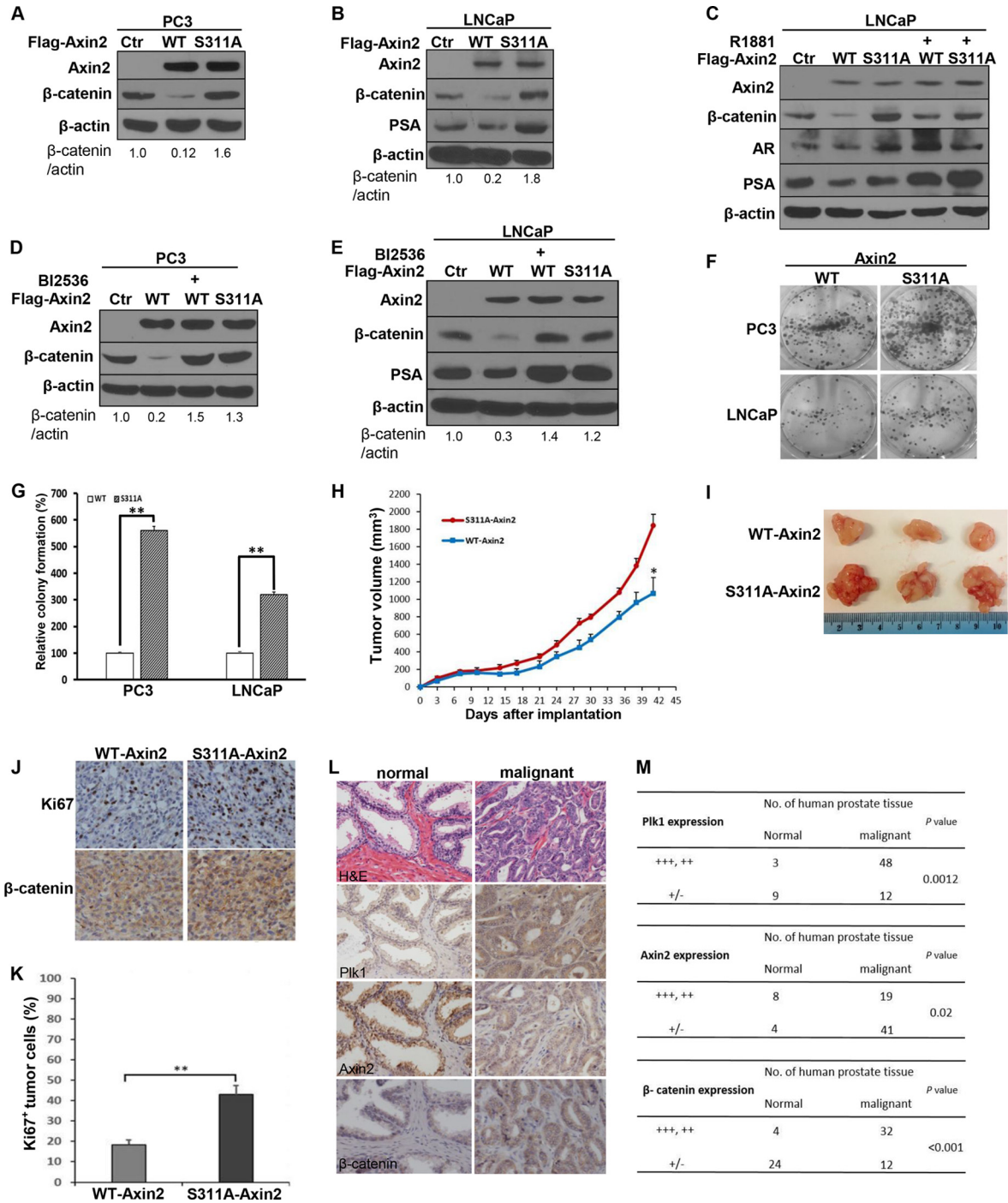


**FIG 6** Plk1 phosphorylation of axin2 mediates degradation of  $\beta$ -catenin in human prostate cancer cells. (A to C) Introduction of the S311A mutation antagonizes axin2 expression-induced degradation of  $\beta$ -catenin. PC3 (A) and LNCaP (B and C) cells were transfected with Flag-axin2 (WT or S311A) constructs for 48 h in the absence (A and B) or presence (C) of R1881. (D and E) Inhibition of Plk1 activity by BI2536 inhibits axin2 expression-induced degradation of  $\beta$ -catenin. PC3 (D) and LNCaP (E) cells were transfected with axin2 (WT or S311A) constructs for 48 h and treated with or without BI2536. (F) Axin2-S311A-expressing cells have a greater colony formation ability than do axin2-expressing cells. PC3 or LNCaP cells ( $2 \times 10^3$ ) expressing axin2 constructs were seeded into plates for 7 days, followed by colony formation assays. (G) Quantification of the colonies in panel F. The bar graph was obtained by calculating the percentages of colonies relative to those of WT-axin2, defined as 100% (means  $\pm$  standard deviations;  $n = 3$  independent experiments). \*\*,  $P < 0.01$ . (H to K) Axin2-expressing PC3 cells show reduced tumor formation ability compared to cells stably expressing axin2-S311A. PC3 cells ( $1 \times 10^6$ ) stably expressing axin2 (WT or S311A) were inoculated into nude mice and grown for 42 days. (H) Tumor sizes were measured every 3 days (means  $\pm$  standard errors of the means;  $n = 4$  mice from each experiment group). \*,  $P < 0.05$ . (I) Images of tumors at the end of the study. (J) Representative images of IHC staining for Ki67 and  $\beta$ -catenin in harvested tumors. (K) Average percentages of Ki67-positive cells from multiple tumor sections. Data represent means  $\pm$  standard errors of the means ( $n = 4$ ). \*\*,  $P < 0.01$ . (L) Expression of Plk1, axin2, and  $\beta$ -catenin in human normal and malignant prostate tissues. (M) Statistical analysis of IHC staining for panel L. “+++ , ++” represents overexpression or high relative expression levels; “+/-” represents negative expression or low relative expression levels.  $P$  values were determined by a  $\chi^2$  test. Western blots in panels A to E are representative of data from three or more experiments.

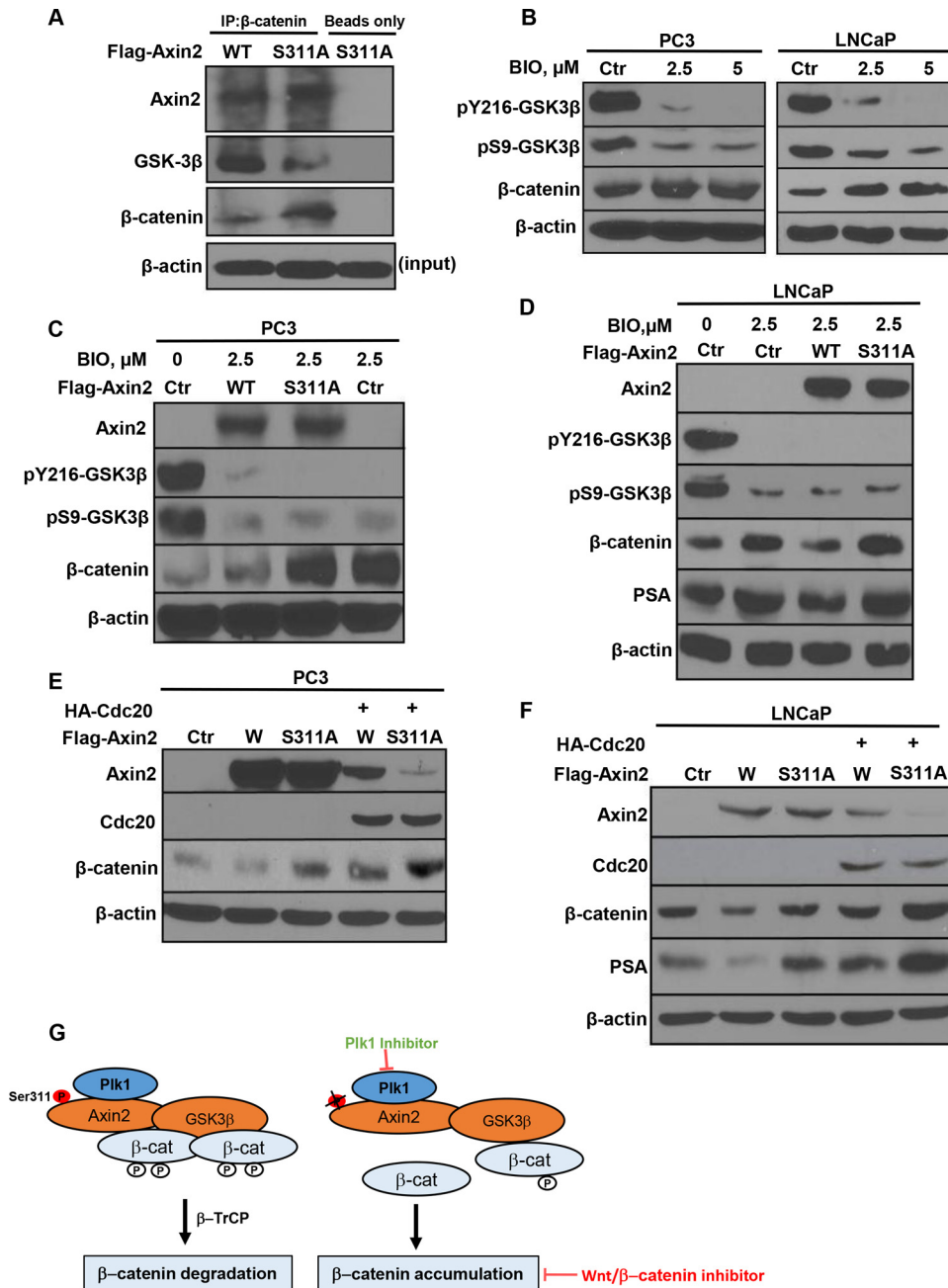


**FIG 7** Plk1 phosphorylation of axin2 enhances binding between GSK3 $\beta$  and  $\beta$ -catenin and inhibits Cdc20-mediated degradation of axin2. (A) Introduction of the axin2-S311 mutation reduces the binding affinity between GSK3 $\beta$  and  $\beta$ -catenin. PC3 cells were transfected with different forms of axin2 (WT or S311A) and subjected to anti- $\beta$ -catenin IP, followed by anti-GSK3 $\beta$  and anti- $\beta$ -catenin IB. (B) Inhibition of GSK3 $\beta$  activity in human prostate cancer cells. PC3 and LNCaP cells were treated with BIO for 48 h and harvested. (C and D) PC3 and LNCaP cells were transfected with axin2 constructs in the presence or absence of BIO. (E and F) Introduction of the S311A mutation renders axin2 more sensitive to Cdc20-mediated degradation. PC3 (E) and LNCaP (F) cells were cotransfected with Flag-axin2 constructs (WT or S311A) and hemagglutinin (HA)-Cdc20 for 48 h and harvested. (G) Proposed working model based on the results of this study.

pathways in human PCa xenograft models (12). Second, among multiple castration-associated side effects, increased oxidative stress contributes to the elevation of Plk1 levels in an NF- $\kappa$ B-dependent manner (15). Third, Plk1 phosphorylation of Clip-170 (37) and p150<sup>Glued</sup> (38), two microtubule plus-end binding proteins, enhances microtubule dynamics, consequently contributing to taxel resistance (39). Fourth, Plk1 phosphorylation of the PTEN tumor suppressor causes its inactivation and, thus, activation of the phosphatidylinositol 3-

nase (PI3K)-AKT-mTOR pathway, a major driving force for PCa progression (40). Fifth, castration-induced elevations of Plk1 levels contribute to the constitutive activation of AR signaling, another major force in CRPC disease. Consequently, Plk1 inhibition enhances the efficacy of androgen signaling blockades in CRPC (15). The data presented here are surprising as they clearly show that one major side effect of inhibiting Plk1 is activation of the Wnt/ $\beta$ -catenin pathway. Inhibition of Plk1-associated activation of Wnt/ $\beta$ -catenin signaling is

not affected by the different genetic backgrounds of PCa cells, including the mutational status of PTEN, p53, and AR (Fig. 1). This is of high clinical significance because PCa is an extremely heterogeneous disease, and identification of the conserved mechanism(s) across different subtypes of PCa will lead to the discovery of more efficient drugs/approaches. Previous studies also linked the Wnt/ $\beta$ -catenin pathway to prostate tumorigenesis (8). Next-generation sequencing studies of CRPC specimens identified the Wnt/ $\beta$ -catenin pathway as a top signaling pathway with significant genomic alterations in CRPC (9). However, how the Wnt/ $\beta$ -catenin pathway can be targeted in CRPC treatment remains unclear. Because Plk1-associated kinase activity is clearly involved in many CRPC treatment-related events, we propose that the combination of Plk1 inhibition and inhibition of the Wnt/ $\beta$ -catenin pathway is a valid treatment approach for CRPC.

**Role of Plk1 in regulation of nonmitotic events.** Plk1 is now recognized as a key regulator in cellular processes with diverse functions (11, 41). For example, we previously reported that Plk1 phosphorylation of Topors and GTSE1, two negative regulators of the p53 tumor suppressor, leads to p53 inactivation (42, 43) and premature termination of cell cycle arrest due to DNA damage. We have also shown that Plk1 phosphorylation of Hbo1 and Orc2, two members of the DNA replication machinery, regulates DNA synthesis by affecting chromatin loading of prereplicative complexes (16, 44). More recently, we discovered that Plk1 phosphorylation of PTEN leads to a tumor-promoting metabolic state with increased glycolysis and glutamine anaplerosis, two hallmarks of cancer cells (40). Of interest, others reported previously that Plk1 interacts with and phosphorylates axin and that Plk1 phosphorylation of axin is involved in proper centrosome formation. Because abnormal amplification of centrosomes leads to chromosome missegregation and aneuploidy, Plk1 phosphorylation of axin could be a contributing factor in cancer development. However, whether Plk1 phosphorylation of axin affects the status of the Wnt/ $\beta$ -catenin pathway is still not known (45). Furthermore, it was recently discovered that Nek2 phosphorylates and stabilizes  $\beta$ -catenin at mitotic centrosomes and that this event, which is critical for bipolar spindle formation in metaphase, acts downstream of Plk1 (46). Therefore, it is clear that the cross talk between Plk1 and the members of  $\beta$ -catenin pathway likely regulates both the canonical Wnt/ $\beta$ -catenin pathway and centrosome function.

In this study, we now identify axin2, another member of the axin protein family, as a novel Plk1 substrate (Fig. 5). Significantly, our studies revealed that Plk1 phosphorylation of axin2 is clearly involved in the regulation of  $\beta$ -catenin stability and, consequently, PCa growth (Fig. 6). Mechanistically, Plk1 phosphorylation of axin2 facilitates the GSK3 $\beta$ -dependent phosphorylation of  $\beta$ -catenin by enhancing binding between GSK3 $\beta$  and  $\beta$ -catenin, an essential early step for the subsequent degradation of  $\beta$ -catenin. In cells expressing the axin2-S311A mutant, binding between GSK3 $\beta$  and  $\beta$ -catenin is significantly reduced, leading to inhibited  $\beta$ -catenin phosphorylation and accumulation of  $\beta$ -catenin protein (Fig. 7G). This novel discovery provides an explanation for how the inhibition of Plk1 leads to the activation of the Wnt/ $\beta$ -catenin pathway.

In AR-negative tumors, although the mechanisms by which prostate cancer cells develop into the androgen-insensitive stage are currently unclear, it is believed that tumor cells must either bypass or adapt the androgen signaling pathway to survive in a low-androgen environment during progression. Thus, in AR-null PC3-derived tumors, activation of  $\beta$ -catenin must activate other

critical downstream targets other than AR to drive tumor growth. In AR-positive and androgen-dependent tumors (LuCaP35CR), Plk1 inhibitor treatment caused  $\beta$ -catenin activation, directly activating AR signaling.

In summary, our findings strongly suggest that activation of the Wnt/ $\beta$ -catenin signaling pathway needs to be carefully considered when Plk1 inhibitors are used in various combination therapies and that targeting inhibition of Plk1 and the Wnt/ $\beta$ -catenin pathway simultaneously would most likely be an improved and more effective approach for future CRPC therapy.

## ACKNOWLEDGMENTS

We thank Robert Vessella for the LuCaP35CR mouse line.

This work was supported by NIH grant R01 CA157429 (X.L.), NIH grant R01 CA124586 (S.F.K.), NIH grant R01 AR059130 (N.A.), NIH grant R01 CA176748 (N.A.), and ACS grant RSG-13-073 (X.L.). Xenograft data were acquired by a Purdue Center for Cancer Research facility supported by grant P30 CA023168.

## REFERENCES

- Schrijvers D, Van Erps P, Cortvriend J. 2010. Castration-refractory prostate cancer: new drugs in the pipeline. *Adv Ther* 27:285–296. <http://dx.doi.org/10.1007/s12325-010-0038-1>.
- Saad F. 2013. Evidence for the efficacy of enzalutamide in postchemotherapy metastatic castrate-resistant prostate cancer. *Ther Adv Urol* 5:201–210. <http://dx.doi.org/10.1177/1756287213490054>.
- Beer TM, Armstrong AJ, Rathkopf DE, Loriot Y, Sternberg CN, Higano CS, Iversen P, Bhattacharya S, Carles J, Chowdhury S, Davis ID, de Bono JS, Evans CP, Fizazi K, Joshua AM, Kim CS, Kimura G, Mainwaring P, Mansbach H, Miller K, Noonberg SB, Perabo F, Phung D, Saad F, Scher HI, Taplin ME, Venner PM, Tombal B. 2014. Enzalutamide in metastatic prostate cancer before chemotherapy. *N Engl J Med* 371:424–433. <http://dx.doi.org/10.1056/NEJMoa1405095>.
- Ryan CJ, Smith MR, de Bono JS, Molina A, Logothetis CJ, de Souza P, Fizazi K, Mainwaring P, Piulats JM, Ng S, Carles J, Mulders PF, Basch E, Small EJ, Saad F, Schrijvers D, Van Poppel H, Mukherjee SD, Suttman H, Gerritsen WR, Flaig TW, George DJ, Yu EY, Efstathiou E, Pantuck A, Winquist E, Higano CS, Taplin ME, Park Y, Kheoh T, Griffin T, Scher HI, Rathkopf DE. 2013. Abiraterone in metastatic prostate cancer without previous chemotherapy. *N Engl J Med* 368:138–148. <http://dx.doi.org/10.1056/NEJMoa1209096>.
- Rathkopf DE, Smith MR, de Bono JS, Logothetis CJ, Shore ND, de Souza P, Fizazi K, Mulders PF, Mainwaring P, Hainsworth JD, Beer TM, North S, Fradet Y, Van Poppel H, Carles J, Flaig TW, Efstathiou E, Yu EY, Higano CS, Taplin ME, Griffin TW, Todd MB, Yu MK, Park YC, Kheoh T, Small EJ, Scher HI, Molina A, Ryan CJ, Saad F. 2014. Updated interim efficacy analysis and long-term safety of abiraterone acetate in metastatic castration-resistant prostate cancer patients without prior chemotherapy (COU-AA-302). *Eur Urol* 66:815–825. <http://dx.doi.org/10.1016/j.eururo.2014.02.056>.
- Ryan CJ, Molina A, Griffin T. 2013. Abiraterone in metastatic prostate cancer. *N Engl J Med* 368:1458–1459. <http://dx.doi.org/10.1056/NEJMc1301594>.
- Clevers H, Nusse R. 2012. Wnt/ $\beta$ -catenin signaling and disease. *Cell* 149:1192–1205. <http://dx.doi.org/10.1016/j.cell.2012.05.012>.
- Yokoyama NN, Shao S, Hoang BH, Mercola D, Zi X. 2014. Wnt signaling in castration-resistant prostate cancer: implications for therapy. *Am J Clin Exp Urol* 2:27–44.
- Grasso CS, Wu YM, Robinson DR, Cao X, Dhanasekaran SM, Khan AP, Quist MJ, Jing X, Lonigro RJ, Brenner JC, Asangani IA, Ateeq B, Chun SY, Siddiqui J, Sam L, Anstett M, Mehra R, Prensner JR, Palanisamy N, Ryslik GA, Vandin F, Raphael BJ, Kunju LP, Rhodes DR, Pienta KJ, Chinnaiyan AM, Tomlins SA. 2012. The mutational landscape of lethal castration-resistant prostate cancer. *Nature* 487:239–243. <http://dx.doi.org/10.1038/nature11125>.
- Weichert W, Schmidt M, Gekeler V, Denkert C, Stephan C, Jung K, Loening S, Dietel M, Kristiansen G. 2004. Polo-like kinase 1 is overexpressed in prostate cancer and linked to higher tumor grades. *Prostate* 60:240–245. <http://dx.doi.org/10.1002/pros.20050>.
- Strebhardt K, Ullrich A. 2006. Targeting polo-like kinase 1 for cancer therapy. *Nat Rev Cancer* 6:321–330. <http://dx.doi.org/10.1038/nrc1841>.

12. Sun Y, Wang B-E, Leong KG, Yue P, Li L, Jhunjhunwala S, Chen D, Seo K, Modrusan Z, Gao WQ, Settleman J, Johnson L. 2012. Androgen deprivation causes epithelial-mesenchymal transition in the prostate: implications for androgen-deprivation therapy. *Cancer Res* 72:527–536. <http://dx.doi.org/10.1158/0008-5472.CAN-11-3004>.
13. Russo MA, Kang KS, Di Cristofano A. 2013. The PLK1 inhibitor GSK461364A is effective in poorly differentiated and anaplastic thyroid carcinoma cells, independent of the nature of their driver mutations. *Thyroid* 23:1284–1293. <http://dx.doi.org/10.1089/thy.2013.0037>.
14. Steegmaier M, Hoffmann M, Baum A, Lenart P, Petronczki M, Krssak M, Gurtler U, Garin-Chesa P, Lieb S, Quant J, Grauert M, Adolf GR, Kraut N, Peters JM, Rettig WJ. 2007. BI 2536, a potent and selective inhibitor of polo-like kinase 1, inhibits tumor growth in vivo. *Curr Biol* 17:316–322. <http://dx.doi.org/10.1016/j.cub.2006.12.037>.
15. Zhang Z, Hou X, Shao C, Li J, Cheng JX, Kuang S, Ahmad N, Ratliff T, Liu X. 2014. Plk1 inhibition enhances the efficacy of androgen signaling blockade in castration-resistant prostate cancer. *Cancer Res* 74:6635–6647. <http://dx.doi.org/10.1158/0008-5472.CAN-14-1916>.
16. Song B, Liu XS, Davis K, Liu X. 2011. Plk1 phosphorylation of Orc2 promotes DNA replication under conditions of stress. *Mol Cell Biol* 31:4844–4856. <http://dx.doi.org/10.1128/MCB.06110-11>.
17. Liu X, Lei M, Erikson RL. 2006. Normal cells, but not cancer cells, survive severe Plk1 depletion. *Mol Cell Biol* 26:2093–2108. <http://dx.doi.org/10.1128/MCB.26.6.2093-2108.2006>.
18. Liu X, Erikson RL. 2003. Polo-like kinase (Plk)1 depletion induces apoptosis in cancer cells. *Proc Natl Acad Sci U S A* 100:5789–5794. <http://dx.doi.org/10.1073/pnas.1031523100>.
19. Dai D, Holmes AM, Nguyen T, Davies S, Theele DP, Verschraegen C, Leslie KK. 2005. A potential synergistic anticancer effect of paclitaxel and amifostine on endometrial cancer. *Cancer Res* 65:9517–9524. <http://dx.doi.org/10.1158/0008-5472.CAN-05-1613>.
20. Chou TC, Talalay P. 1984. Quantitative analysis of dose-effect relationships: the combined effects of multiple drugs or enzyme inhibitors. *Adv Enzyme Regul* 22:27–55. [http://dx.doi.org/10.1016/0065-2571\(84\)90007-4](http://dx.doi.org/10.1016/0065-2571(84)90007-4).
21. Bello D, Webber MM, Kleinman HK, Wartinger DD, Rhim JS. 1997. Androgen responsive adult human prostatic epithelial cell lines immortalized by human papillomavirus 18. *Carcinogenesis* 18:1215–1223. <http://dx.doi.org/10.1093/carcin/18.6.1215>.
22. Raab M, Kappel S, Kramer A, Sanhaji M, Matthes Y, Kurunci-Csacsko E, Calzada-Wack J, Rathkolb B, Rozman J, Adler T, Busch DH, Esposito I, Fuchs H, Gailus-Durner V, Klingenspor M, Wolf E, Sanger N, Prinz F, Angelis MH, Seibler J, Yuan J, Bergmann M, Knecht R, Kreft B, Strebhardt K. 2011. Toxicity modelling of Plk1-targeted therapies in genetically engineered mice and cultured primary mammalian cells. *Nat Commun* 2:395. <http://dx.doi.org/10.1038/ncomms1395>.
23. Kuruma H, Matsumoto H, Shiota M, Bishop J, Lamoureux F, Thomas C, Briere D, Los G, Gleave M, Fanjul A, Zoubeidi A. 2013. A novel antiandrogen, compound 30, suppresses castration-resistant and MDV3100-resistant prostate cancer growth in vitro and in vivo. *Mol Cancer Ther* 12:567–576. <http://dx.doi.org/10.1158/1535-7163.MCT-12-0798>.
24. Gilmartin AG, Bleam MR, Richter MC, Erskine SG, Kruger RG, Madden L, Hassler DF, Smith GK, Gontarek RR, Courtney MP, Sutton D, Diamond MA, Jackson JR, Laquerre SG. 2009. Distinct concentration-dependent effects of the polo-like kinase 1-specific inhibitor GSK461364A, including differential effect on apoptosis. *Cancer Res* 69:6969–6977. <http://dx.doi.org/10.1158/0008-5472.CAN-09-0945>.
25. Yim H. 2013. Current clinical trials with polo-like kinase 1 inhibitors in solid tumors. *Anticancer Drugs* 24:999–1006. <http://dx.doi.org/10.1097/CAD.000000000000007>.
26. Corey E, Quinn JE, Buhler KR, Nelson PS, Macoska JA, True LD, Vessella RL. 2003. LuCaP 35: a new model of prostate cancer progression to androgen independence. *Prostate* 55:239–246. <http://dx.doi.org/10.1002/pros.10198>.
27. Mostaghel EA, Marck BT, Plymate SR, Vessella RL, Balk S, Matsumoto AM, Nelson PS, Montgomery RB. 2011. Resistance to CYP17A1 inhibition with abiraterone in castration-resistant prostate cancer: induction of steroidogenesis and androgen receptor splice variants. *Clin Cancer Res* 17:5913–5925. <http://dx.doi.org/10.1158/1078-0432.CCR-11-0728>.
28. Iliuk A, Liu XS, Xue L, Liu X, Tao WA. 2012. Chemical visualization of phosphoproteomes on membrane. *Mol Cell Proteomics* 11:629–639. <http://dx.doi.org/10.1074/mcp.O112.018010>.
29. MacDonald BT, Tamai K, He X. 2009. Wnt/beta-catenin signaling: components, mechanisms, and diseases. *Dev Cell* 17:9–26. <http://dx.doi.org/10.1016/j.devcel.2009.06.016>.
30. Lee E, Madar A, David G, Garabedian MJ, Dasgupta R, Logan SK. 2013. Inhibition of androgen receptor and beta-catenin activity in prostate cancer. *Proc Natl Acad Sci U S A* 110:15710–15715. <http://dx.doi.org/10.1073/pnas.1218168110>.
31. Truica CI, Byers S, Gelmann EP. 2000. Beta-catenin affects androgen receptor transcriptional activity and ligand specificity. *Cancer Res* 60:4709–4713.
32. Verras M, Brown J, Li X, Nusse R, Sun Z. 2004. Wnt3a growth factor induces androgen receptor-mediated transcription and enhances cell growth in human prostate cancer cells. *Cancer Res* 64:8860–8866. <http://dx.doi.org/10.1158/0008-5472.CAN-04-2370>.
33. Salas TR, Kim J, Vakar-Lopez F, Sabichi AL, Troncoso P, Jenster G, Kikuchi A, Chen SY, Shemshedini L, Suraokar M, Logothetis CJ, DiGiovanni J, Lippman SM, Menter DG. 2004. Glycogen synthase kinase-3 beta is involved in the phosphorylation and suppression of androgen receptor activity. *J Biol Chem* 279:19191–19200. <http://dx.doi.org/10.1074/jbc.M309560200>.
34. Sharma M, Chuang WW, Sun Z. 2002. Phosphatidylinositol 3-kinase/Akt stimulates androgen pathway through GSK3beta inhibition and nuclear beta-catenin accumulation. *J Biol Chem* 277:30935–30941. <http://dx.doi.org/10.1074/jbc.M201919200>.
35. Wang L, Lin HK, Hu YC, Xie S, Yang L, Chang C. 2004. Suppression of androgen receptor-mediated transactivation and cell growth by the glycogen synthase kinase 3 beta in prostate cells. *J Biol Chem* 279:32444–32452. <http://dx.doi.org/10.1074/jbc.M313963200>.
36. Hadjihannas MV, Bernkopf DB, Bruckner M, Behrens J. 2012. Cell cycle control of Wnt/beta-catenin signalling by conductin/axin2 through CDC20. *EMBO Rep* 13:347–354. <http://dx.doi.org/10.1038/embor.2012.12>.
37. Li H, Liu XS, Yang X, Wang Y, Wang Y, Turner JR, Liu X. 2010. Phosphorylation of CLIP-170 by Plk1 and CK2 promotes timely formation of kinetochore-microtubule attachments. *EMBO J* 29:2953–2965. <http://dx.doi.org/10.1038/emboj.2010.174>.
38. Li H, Liu XS, Yang X, Song B, Wang Y, Liu X. 2010. Polo-like kinase 1 phosphorylation of p150Glued facilitates nuclear envelope breakdown during prophase. *Proc Natl Acad Sci U S A* 107:14633–14638. <http://dx.doi.org/10.1073/pnas.1006615107>.
39. Hou X, Li Z, Huang W, Li J, Staiger C, Kuang S, Ratliff T, Liu X. 2013. Plk1-dependent microtubule dynamics promotes androgen receptor signaling in prostate cancer. *Prostate* 73:1352–1363. <http://dx.doi.org/10.1002/pros.22683>.
40. Li Z, Li J, Bi P, Lu Y, Burcham G, Elzey BD, Ratliff T, Konieczny SF, Ahmad N, Kuang S, Liu X. 2014. Plk1 phosphorylation of PTEN causes a tumor-promoting metabolic state. *Mol Cell Biol* 34:3642–3661. <http://dx.doi.org/10.1128/MCB.00814-14>.
41. Liu X. 2015. Targeting Polo-like kinases: a promising therapeutic approach for cancer treatment. *Transl Oncol* 8:185–195. <http://dx.doi.org/10.1016/j.tranon.2015.03.010>.
42. Liu XS, Li H, Song B, Liu X. 2010. Polo-like kinase 1 phosphorylation of G2 and S-phase-expressed 1 protein is essential for p53 inactivation during G2 checkpoint recovery. *EMBO Rep* 11:626–632. <http://dx.doi.org/10.1038/embor.2010.90>.
43. Yang X, Li H, Liu XS, Deng A, Liu X. 2009. Cdc2-mediated phosphorylation of CLIP-170 is essential for its inhibition of centrosome reduplication. *J Biol Chem* 284:28775–28782. <http://dx.doi.org/10.1074/jbc.M109.017681>.
44. Song B, Liu XS, Rice SJ, Kuang S, Elzey BD, Konieczny SF, Ratliff TL, Hazbun T, Chiorean EG, Liu X. 2013. Plk1 phosphorylation of orc2 and hbo1 contributes to gemcitabine resistance in pancreatic cancer. *Mol Cancer Ther* 12:58–68. <http://dx.doi.org/10.1158/1535-7163.MCT-12-0632>.
45. Ruan K, Ye F, Li C, Liou YC, Lin SC, Lin SY. 2012. PLK1 interacts and phosphorylates Axin that is essential for proper centrosome formation. *PLoS One* 7:e49184. <http://dx.doi.org/10.1371/journal.pone.0049184>.
46. Mbom BC, Siemers KA, Ostrowski MA, Nelson WJ, Barth AI. 2014. Nek2 phosphorylates and stabilizes beta-catenin at mitotic centrosomes downstream of Plk1. *Mol Biol Cell* 25:977–991. <http://dx.doi.org/10.1091/mbc.E13-06-0349>.